JCTC Journal of Chemical Theory and Computation

Article

pubs.acs.org/JCTC

Self-Assembly of Triblock Janus Nanoparticle in Nanotube

Noriyoshi Arai,*[,†] Kenji Yausoka,*[,‡] and Xiao Cheng Zeng*[,§]

[†]Department of Mechanical Engineering and Intelligent Systems, University of Electro-Communications, Chofu, Tokyo, Japan

[‡]Department of Mechanical Engineering, Keio University, Yokohama, Japan

[§]Department of Chemistry, Univeristy of Nebraska—Lincoln, Lincoln, Nebraska, United States

Supporting Information

ABSTRACT: We have performed molecular simulations to investigate morphologies and the phase diagram of the self-assembled triblock Janus nanoparticle confined to nanotubes. The triblock Janus nanoparticle is decorated with two hydrophobic caps at the north and south poles with a tunable area, separated by an electrically charged middle band. On the basis of the observed pressure- and tube-radius-dependent morphologies, we derive semiquantitative phase diagrams of the axial pressure versus the ratio of the radius of the nanoparticle to the radius of the nanotube. Three distinct walls of the nanotube, namely, hydrophobic, hydrophilic, and hydroneutral, are considered. We find that the three phase diagrams corresponding to three chemically different walls of the nanotube show some universal features. These features can be illustrated through a schematic assembly map and a roadmap on the variation of coordination number of the nanoparticles. In particular, we find that highly ordered morphologies tend to form when the coordination number of Janus particles is a multiple of 2. The orientation ordering and self-assembly behavior of the Janus nanoparticles can be qualitatively predicted when the chemical nature of the nanotube wall is known.

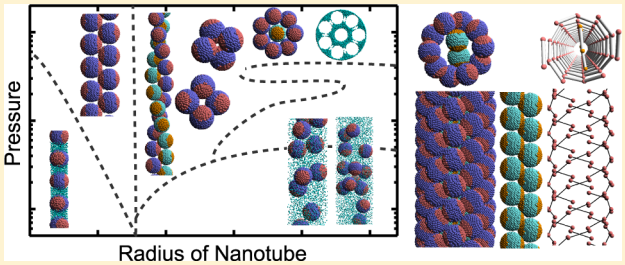

INTRODUCTION

Self-assembly of colloidal nanoparticles is a widely used synthetic method to fabricate nanostructured materials. Novel self-assembled materials can be exploited for applications such as optical sensors,[1,2] photonic crystals,[3,4] and quantum dots,[5,6] among many others. Hence, understanding and controlling the self-assembly processes of colloidal nanoparticles has received considerable attention in materials chemistry and engineering. One useful strategy to control morphologies of self-assembled nanoparticles is to design colloidal particles with anisotropic shapes and interactions.[7−10] It is known that anisotropic particles can self-assemble into complex structures or form ordered phases.[11,12] Highly ordered assemblies may entail new electronic and optical properties that may not be available in other assemblies.[13,14]

The Janus nanoparticle (JNP) is a unique anisotropic nanoparticle that typically has two or more distinct functional surface regions. With two different chemical and/or physical properties distributed among different surface regions of a single JNP, new characteristics arise for the self-assembled JNPs. Suci et al.[15] synthesized a streptavidin (StAv)-functionalized protein cage that can serve as a "plug and play" nanoplatform for coupling with a biotinylated functional group. The resulting StAv-functionalized Janus particles may be used to control the orientation of nanoplatforms targeted to the cell surface, thereby offering a possibility as multifunctional drug carriers. Cole-Hamilton[16] suggested that JNPs can be used as phase transfer catalysts owing to the large interfacial area between JNPs and the aqueous phase for the reaction, short reaction times, and the simple separation process required for recovering solid catalysts. Jiang et al.[17] demonstrated that a JNP with a hemisurface coated by metal behaves like a microrotor under laser irradiation. The motion is caused by absorption of a laser at the metallic side of the JNP, which creates a local temperature gradient.

Previous studies have shown that amphiphilic JNPs can self-assemble spontaneously, forming a variety of self-organized nanostructures such as a bilayer, hexagonal crystals, and a Kagome lattice,[18−22] depending on the surface properties and anisotropy of JNP, as well as the temperature. Nevertheless, preparation of JNPs with a controlled size and structure in large quantities is still a challenge. Recently, several synthesis strategies, e.g., electrohydrodynamic cojetting[23] and self-organized precipitation,[24] have been developed to synthesize novel JNPs.[25] Chen et al.[18] succeeded in the fabrication of triblock Janus spheres by sequential glancing angle deposition[26] of gold coating. The triblock JNPs decorated with two hydrophobic caps separated by an electrically charged middle band are allowed to deposit as sediment in deionized solvent. The self-assembled JNPs give rise to an open Kagome structure in aqueous NaCl solutions, contrary to the close-packed periodic arrangements of the spheres.

Received: September 6, 2012
Published: December 19, 2012

   dx.doi.org/10.1021/ct3007748 | J. Chem. Theory Comput. 2013, 9, 179−187

It is also known that fluids confined to nanoscale channels can exhibit new phases not seen in the bulk.[27,28] Even for simple fluids such as water, abnormal dynamical behavior has been observed due to the nanoscale confinement.[29,30] When complex fluids are confined to nanoscale channels, the shear viscosity and morphology of fluids can be significantly affected by chemical conditions of the confining surfaces.[31] Moreover, richer morphologies of self-assembled JNPs are expected when confined to a nanotube, not only because the dimensional constraint imposed by the nanotube can affect the thermodynamic equilibrium but also because the added distinctive chemical interactions between the nanotube, solvent, hydrophilic band, and hydrophobic poles will definitely disrupt the existing force balance in the free solution. The goal of this computational study is to investigate the phase behavior of self-assembled triblock JNPs in different types of nanotubes. To our knowledge, a simulation study of morphologies of JNPs has not been reported in the literature.

METHOD AND MODEL

Simulation Method. We employ the dissipative particle dynamics (DPD) simulation method[32,33] to study the phase behavior of a confined JNP solution. The DPD method allows the simulation being carried out on a *millisecond* time scale and *micrometer* length scale since only the motion of coarse-grained particles (composed of a group of atoms or molecules) is simulated. The fundamental equation in the DPD method is still Newton's equation of motion. For a particle i, each DPD bead is subject to three types of forces: conservative, dissipative, and random. Note that each JNP is treated as a rigid body.[34] Hence, all DPD beads within the same JNP have the same translational velocity, and the intra-JNP forces will not be included in Newton's equation of motion. Newton's equation of motion for the particle i is given as follows:

$$m_i \frac{d\mathbf{v}_i}{dt} = \mathbf{f}_i = \sum_{j\neq i} \mathbf{F}_{ij}^{C} + \sum_{j\neq i} \mathbf{F}_{ij}^{D} + \sum_{j\neq i} \mathbf{F}_{ij}^{R} \quad (1)$$

where m is the mass, $\mathbf{v}$ the velocity, $\mathbf{F}^C$ the conservative force, $\mathbf{F}^R$ the pairwise random force, and $\mathbf{F}^D$ the dissipative force. The force acting on the JNP is summed over all the interbead forces between particles i and j. The conservative force is softly repulsive and is given by

$$\mathbf{F}_{ij}^{C} = \begin{cases} -a_{ij}\left(1 - \frac{|\mathbf{r}_{ij}|}{r_c}\right)\mathbf{n}_{ij}, & |\mathbf{r}_{ij}| \le r_c \\ 0, & |\mathbf{r}_{ij}| > r_c \end{cases} \quad (2)$$

where $\mathbf{r}_{ij} = \mathbf{r}_j - \mathbf{r}_i$ and $\mathbf{n}_{ij} = \mathbf{r}_{ij}/|\mathbf{r}_{ij}|$. Here, a_{ij} is a parameter to determine the magnitude of the repulsive force between particles i and j, and r_c is the cutoff distance. Random force ($\mathbf{F}_{ij}^R$) and dissipative force ($\mathbf{F}_{ij}^D$) are given by

$$\mathbf{F}_{ij}^{R} = \begin{cases} \sigma\omega^{R}(|\mathbf{r}_{ij}|)\zeta_{ij}\Delta t^{-1/2}\mathbf{n}_{ij}, & |\mathbf{r}_{ij}| \le r_c \\ 0, & |\mathbf{r}_{ij}| > r_c \end{cases} \quad (3)$$

and

$$\mathbf{F}_{ij}^{D} = \begin{cases} -\gamma\omega^{D}(|\mathbf{r}_{ij}|)(\mathbf{n}_{ij}\cdot\mathbf{v}_{ij})\mathbf{n}_{ij}, & |\mathbf{r}_{ij}| \le r_c \\ 0, & |\mathbf{r}_{ij}| > r_c \end{cases} \quad (4)$$

respectively, where $\mathbf{v}_{ij} = \mathbf{v}_j - \mathbf{v}_i$, σ is the noise parameter, γ the friction parameter, Δt is the time step, and ζ_{ij} a random number based on the Gaussian distribution. Here, ω^R and ω^D are r-dependent weight functions which are given by

$$\omega^{D}(r) = [\omega^{R}(r)]^2 = \begin{cases} \left[1 - \frac{|\mathbf{r}_{ij}|}{r_c}\right]^2, & |r_{ij}| \le r_c \\ 0, & |r_{ij}| > r_c \end{cases} \quad (5)$$

The temperature is controlled by a combination of dissipative and random forces. The noise parameter σ and friction parameter γ are connected to each other by the fluctuation–dissipation theorem in the following equation:

$$\sigma^2 = 2\gamma k_B T \quad (6)$$

where k_B is the Boltzmann constant and T is the temperature.

The DPD method has been proven to be very effective by many researches to investigate the dynamics of soft matter at the mesoscopic level, for example, polymer-brush bilayers with colloidal inclusions,[35] colloidal crystallization of gold nanoparticles,[36,37] and human blood.[38] The mesoscopic dynamics of soft matter cannot be handled by the classical molecular dynamics due to limited length and time scale.

Simulation Model and Conditions. For the DPD simulations of the quasi-one-dimensional (Q1D) nanotube system, the periodic boundary condition is applied in the axial (z) direction. Here, Q1D systems mean that systems of particles in domains which are of infinite extent in one direction and of uniformly bounded size in all other directions, like a carbon nanowire and a carbon nanotube. In Figure 1, a model triblock JNP used in the DPD simulation is illustrated. The JNP is composed of both hydrophobic and hydrophilic DPD beads on a diamond lattice with a lattice constant α = 0.47 nm. Each JNP consists of 1684 DPD beads: 524 are hydrophobic (labeled by the letter A) and another 1160 are hydrophilic (labeled by the letter B). The radius of the JNP R_{NP} is 1.94 nm. The solvent bead (or monomer) is labeled by the letter S. The interaction parameters between any two DPD beads are shown in Table 1.

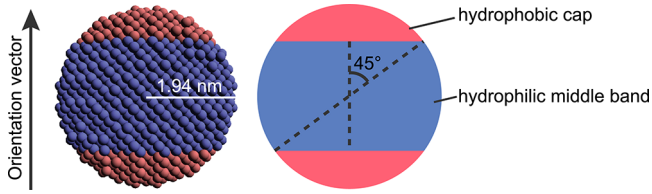

Figure 1. Triblock Janus nanoparticle (JNP) model in the DPD simulations. The orientational vector of a triblock JNP is marked by a left arrow, i.e., the line from the pole of one hydrophobic cap to another pole of the hydrophobic cap. A schematic view of JNP is given on the right. The angle between the orientational vector and the diagonal line of hydrophobic caps is 45°.

Table 1. Interaction Parameters a_{ij} (in k_BT unit) between Bead Pairs in eq 2

	A	B	S
A	10	50	100
B	50	25	25
S	100	25	25

dx.doi.org/10.1021/ct3007748 | J. Chem. Theory Comput. 2013, 9, 179–187

Note that the interaction parameter between two solvent beads is set with the same value (25 k_BT) when the number of density of solvent is 3.0 in Groot–Warren theory.[39] As such, the interaction parameters a_{AS} (= 100 k_BT > a_{SS}) and a_{BS} (= 25 k_BT = a_{SS}) represent hydrophobic and hydrophilic interaction, respectively. To confirm that this model system is physically sensible, we first performed a test simulation for a confined solution within a nanoscale slit. We found that a stable Kagome lattice structure (Figure S1a) can be kept for a long period of time (~2 μs). Moreover, the crystallization process of the Kagome lattice starting from a random initial configuration can be analyzed by computing the fraction of chain-like bonding in the system as a function of time (Figure S1b). These results are consistent with a recent experiment.[18]

The inner surface of a cylindrical nanotube is treated as a smooth wall as in our previous study.[40] The force field of the smooth wall is derived on the basis of a structured wall by summing the DPD forces between every pair of DPD bead and wall bead.[27] Integration of the sum results in a force function between the DPD bead and the smooth wall (within the cutoff distance r_c), that is,

$$\mathbf{F}_{wall}(R) = \frac{1}{6}\pi\rho_{wall}a_{wall,p}(-R^4 + 2R^3 - 2R + 1)\mathbf{R}/R \quad (7)$$

where ρ_{wall} is the number density of the structured wall, $a_{wall,p}$ is the interaction parameter between the wall and the DPD bead, $\mathbf{R}$ is the normal vector from the bead to the wall surface, and thus $R = |\mathbf{R}|$ is the distance between the wall and the bead. We have considered eight different radii for the nanotube, R_{NT}/R_{NP} = 1.1, 1.5, 2.0, 2.5, 3.0, 3.167, 3.333, and 3.5. Here, R_{NT} is the radius of the nanotube. To avoid undesirable penetration of solvent beads into the wall of the nanotube at high axial pressure, ρ_{wall} is chosen to be 10.0, twice as large as that used in our previous study.[41] The interaction parameters between the nanotube wall and DPD bead are shown in Table 2. Here, the

Table 2. Interaction Parameters $a_{wall,p}$ (in k_BT unit) between Bead and Nanotube Wall in eq 7

	A	B	S
hydrophobic wall	25	75	75
hydrophilic wall	75	25	25
hydroneutral wall	50	50	50

total number of beads in the supercell is 47 298, among which 40 416 beads are for the construction of the JNPs. So there are in total 24 JNPs in the system. The remaining 6882 beads are for the solvent. Thus, the ratio of the number of JNPs to the number of solvent beads is 0.003478, while the mole fraction of JNPs is 0.3475%. The latter can be used as a measure of JNP concentration in the system.

The DPD simulations are performed in the constant-axial pressure P_z and constant-temperature ensemble.[42] It is expected that by increasing P_z, a more ordered morphology of JNPs may be observed. For example, in a previous classical molecular dynamics simulation of water, Bai et al.[43] showed that helical nanoices can form spontaneously in carbon nanotubes at high axial pressure. Also, Melle-Franco and Zerbetto[44] performed a molecular dynamics simulation of the ejection dynamics of an argon liquid from the carbon nanotube under a high axial pressure. A novel phenomenon of laminar flux was observed. In this study, we demonstrate that ordered structures of JNPs and order–disorder transitions can be achieved at high P_z. In the ensuing simulation, the axial pressure is increased stepwise from 0.009 to 1.68 MPa. At each given P_z, 176 ns simulations are carried out, respectively. The temperature is set to 1.0 k_BT. The method developed by Groot and Rabone for scaling the length and time units is adopted.[45] Note that our DPD simulation employs a soft potential for DPD beads. So unphysical overlap among DPD beads can occur under extremely high pressure. We have examined the pressure range (0.009 to 1.68 MPa) used in this study and confirmed that an excluded volume effect is observed under a high pressure (1.5 MPa). Hence, the unphysical bead-overlapping behavior does not occur in our simulation.

Orientational Order Parameter. The orientational vector of the triblock JNP is defined as the line from the pole of the hydrophobic cap to the opposing pole of the hydrophobic cap (see the arrow in Figure 1). The orientational order parameter S is given by

$$S = \frac{1}{2}\langle 3\cos^2\theta - 1\rangle \quad (8)$$

where θ is the angle between the orientational vector and the axial direction. Hence, when the central hydrophilic band of JNPs is in contact with the nanotube wall, $S \sim 1.0$, and when the pole of the hydrophobic cap of JNPs is in contact with the nanotube wall, $S \sim -0.5$.

RESULTS AND DISCUSSION

Hydrophobic Wall. In the first series of DPD simulations, we have investigated the phase behavior of triblock JNPs and solvent confined to a hydrophobic nanotube. In Figure 2, we show a qualitative phase diagram of the system, including representative snapshots of equilibrium morphologies as insets. The vertical axis is P_z, and the horizontal axis is a ratio, R_{NT}/R_{NP}, of the radius of JNP to the radius of the nanotube. The phase boundaries are drawn schematically.

Under strong confinement ($R_{NT}/R_{NP} \leq 1.5$), JNPs tend to disperse in a single-file fashion within the nanotube at relatively low axial pressures. In the strong confinement limit, R_{NT}/R_{NP} = 1.1, both hydrophobic caps of JNPs are in contact with the inner wall of the nanotube (Figure 2a1), while at R_{NT}/R_{NP} = 1.5, only one of the hydrophobic caps is in direct contact with the inner wall (Figure 2a2). As P_z increases, JNPs can interact more strongly with each other, and the orientational vector of JNPs tends to be along the axial direction. As a result, a JNP polymer chain is formed, which links all JNPs through their hydrophobic caps as shown in Figure 2b.

For $R_{NT}/R_{NP} \geq 2.0$ and at relatively low pressure (P_z < 0.05 MPa), JNPs have a larger room to access within the nanotube (see Figure 2c1 and c2) and thus behave like a Q1D liquid, although the diffusion constant is a just a fraction of the diffusion constant in bulk solution (1/2–1/3 in the axial direction and 1/10–1/250 in the radial direction) due to the lateral confinement. In Figure 2, $R_{NT}/R_{NP} \sim 2.0$ can be viewed as a phase boundary between the single-file dispersion and Q1D liquid. At relatively higher pressure ($P_z \geq 0.02$), a double helix structure is observed (Figure 2d). This is because a liable orientation of JNP is compatible with the R_{NP}. In the hydrophobic nanotube, JNP orientational vectors tend to point in the direction normal to the axial direction while their hydrophobic caps are in contact with the inner wall. When P_z is ~0.072 MPa, JNPs aggregate into a double helix as shown in Figure 2d. As P_z further increases to about 0.2 MPa, the double helix is transformed to a triple helix (Figure 2e) while one of

dx.doi.org/10.1021/ct3007748 | J. Chem. Theory Comput. 2013, 9, 179–187

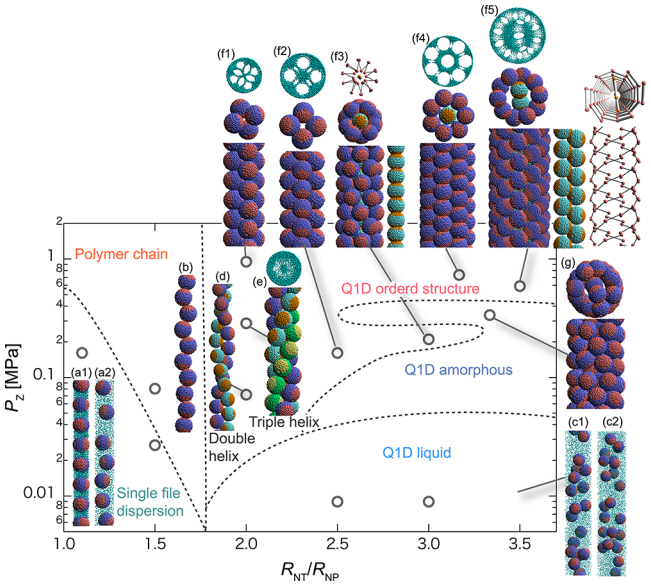

Figure 2. A schematic phase diagram for the triblock JNP solution confined to hydrophobic nanotubes. The vertical axis is the pressure in the axial direction P_z, and the horizontal axis is a ratio, R_{NT}/R_{NP}, of the radius of JNP to the radius of the nanotube. Insets a–f: Representative snapshots of equilibrium morphologies of the triblock JNP solution (nanotube not shown in the figure). (a1 and a2) Single file dispersion: side views for R_{NT}/R_{NP} = 1.1 and P_z = 0.161 MPa, and R_{NT}/R_{NP} = 1.5 and P_z = 0.027 MPa, respectively. (b) Polymer chain: a side view for R_{NT}/R_{NP} = 1.5 and P_z = 0.081 MPa. (c1 and c2) Quasi-1D liquid: side views for R_{NT}/R_{NP} = 2.5 and P_z = 0.009 MPa, and R_{NT}/R_{NP} = 3.5 and P_z = 0.009 MPa, respectively. (d) Double helix: a side view for R_{NT}/R_{NP} = 2.0 and P_z = 0.072 MPa. (e) Triple helix: the top panel is a top view of only solvent, and the bottom panel is a side view for R_{NT}/R_{NP} = 2.0 and P_z = 0.286 MPa. (f1–f5) Quasi-1D ordered structure. (f1) Cross-line close-packed Q1D crystal: The top panel is a top view of only the solvent. The middle panel is a top view. The bottom panel is a side view for R_{NT}/R_{NP} = 2.0 and P_z = 0.949 MPa. (f2) Q1D tetragonal crystal: The top panel is a top view of only the solvent. The middle panel is a top view. The bottom panel is a side view for R_{NT}/R_{NP} = 2.5 and P_z = 0.161 MPa. (f3) Q1D core/sheath structure with a central JNP chain: The top panel is a top view of only orientational vectors of JNPs. The middle panel is a top view. The bottom panel is a side view for R_{NT}/R_{NP} = 3.0 and P_z = 0.215 MPa. (f4) Heptagonal crystal with a central JNP chain: The top panel is a top view of only the solvent. The middle panel is a top view. The bottom panel is a side view for R_{NT}/R_{NP} = 3.167 and P_z = 0.734 MPa. (f5) Helical octahedron crystal: The top panel is a top view of only the solvent. The middle-left panel is a top view. The bottom-left panel is a side view, The bottom-middle panels is a side view with JNPs in the sheath being excluded. The top-right panel is a top view of only orientational vectors of JNPs. The bottom-right panel is a side view of only orientational vectors for R_{NT}/R_{NP} = 3.5 and P_z = 0.591 MPa. (g) Q1D amorphous phase: The top panel is a top view, and the bottom panel is a side view for R_{NT}/R_{NP} = 3.167 and P_z = 0.340 MPa. Color code: solvent molecules in cyan; the hydrophilic groups in blue, blue-green, and green; and the hydrophobic groups in red, orange, and yellow.

two hydrophobic caps of each JNP is still contact with the inner wall. To investigate whether a favorable twisting direction exists for the helix structures, we performed 10 independent simulations at the same state point in the phase diagram. We find that the probability for the clockwise and anticlockwise helix structure is nearly the same, indicating that the direction of the helix structure only depends on the initial configuration or fluctuations. With $P_z \sim 1.0$ MPa, JNPs are alternately piled up in pairs along the axial direction to form a nanowire (we name it the cross-line close-packed Q1D crystal; see Figure 2f1). A top view of the JNP nanowire shows eight apparent JNP domains separated by solvent molecules, where the solvent molecule can be trapped in the central region of the JNP nanowire during a comparatively long time. In the case of the triple helix, however, the density of the solvent is actually lower in the center region (see cyan curves in Figure S2). On the other hand, when P_z < 0.02 MPa, JNPs do not form any ordered morphology and behave like a Q1D liquid. As an indicator of the phase transition from a Q1D liquid to triple helix as P_z increases beyond 0.02 MPa, we find the orientation order parameter S becomes ~0.5 after the phase transition and the corresponding orientational vectors of JNPs turn to radial direction.

For $R_{NT}/R_{NP} \geq 2.5$, the Q1D amorphous phase appears in the axial pressure range of 0.05 < P_z < 0.4 MPa. In this pressure range, JNPs tend to aggregate into a solid-like cluster without long-range order (Figure 2g). As P_z increases beyond 0.4 MPa, various ordered assemblies are observed, as shown in Figure 2f2–f5. Figure 2f2 exhibits a Q1D tetragonal crystal; this structure is composed of four straight polymer chains. The orientational vector of each JNP aligns about 30° to the axial direction. For $R_{NT}/R_{NP} \geq 3.0$ (nanotube with relatively large radius), a Q1D core/sheath structure is formed, where the inner core is either a straight polymer chain (Figure 2f3,f4) or a zigzag double-chain polymer (Figure 2f5). In Figure 2f3, the orientational vector of JNPs of the sheath (red and blue spheres) is perpendicular to the axial direction as one hydrophobic cap is in contact with the inner wall of the nanotube. The orientational vector of JNPs of the core structure (orange and green spheres) is parallel to the axial direction. The coexistence of both normal and parallel orientational vectors is illustrated by the top panel of Figure 2f3. Such a complex configuration of orientational vectors can influence other physical properties of assemblies, for example, leading to dielectric anisotropy and absorption anisotropy.

When P_z > 0.6 MPa, even JNPs in the outer sheath can be bonded with each other. As such, their hydrophobic caps can no longer be in contact with the inner wall of the nanotube (see Figure 2f4 and f5). Indeed, the orientational vector of JNPs depends on both R_{NT}/R_{NP} and P_z, as clearly demonstrated by two Q1D ordered structures: (1) a heptagonal crystal with an inner polymer chain (Figure 2f4) and (2) a helical outer layer with an inner zigzag double-chain polymer (Figure 2f5). For the former structure, the orientational vector of JNPs is parallel to the axial direction, whereas that for the latter structure exhibits multiple directions: the inner zigzag double-chain is perpendicular to the axial direction, while the orientational vectors of JNPs in the outer helical layer line up about 60–70° from the axial direction.

Hydrophilic Wall. In the second series of DPD simulations, hydrophilic nanotubes are considered. In Figure 3, we show a qualitative phase diagram of the system, including representative snapshots of equilibrium morphologies as insets.

In the hydrophilic nanotube, solvent particles prefer to be in contact with the inner wall of the nanotube, and so does the hydrophilic middle band of JNPs. Therefore, the orientational vector of JNPs tends to be parallel to the axial direction. As in the case of the hydrophobic nanotube, a morphology transition from single-file dispersion to the polymer chain occurs at R_{NT}/R_{NP} > 1.5. Under the strong confinement (R_{NT}/R_{NP} = 1.1), the orientational vector of JNPs is parallel to the axial direction (Figure 3a1). Hence, the orientational order parameter S is ~1.

dx.doi.org/10.1021/ct3007748 | J. Chem. Theory Comput. 2013, 9, 179–187

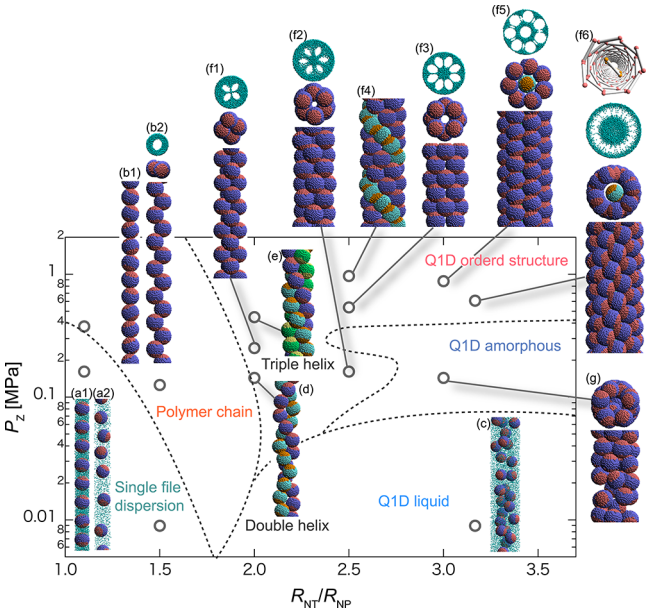

Figure 3. A schematic phase diagram for the triblock JNP solution confined to hydrophilic nanotubes. Insets a−f: Representative snapshots of equilibrium morphologies of the triblock JNP solution (nanotube not shown in the figure). (a1 and a2) Single file dispersion: side views for R_{NT}/R_{NP} = 1.1 and P_z = 0.161 MPa, and R_{NT}/R_{NP} = 1.5 and P_z = 0.009 MPa, respectively. (b1 and b2) Polymer chain: The left panel is a side view. The top panel is a top view of only the solvent. The top-middle panel is a top view. The top-bottom panel is a side view for R_{NT}/R_{NP} = 1.1 and P_z = 0.376 MPa, and R_{NT}/R_{NP} = 1.5 and P_z = 0.125 MPa, respectively. (c) Quasi-1D liquid: a side view for R_{NT}/R_{NP} = 3.167 and P_z = 0.009 MPa. (d) Double helix: a side view for R_{NT}/R_{NP} = 2.0 and P_z = 0.143 MPa. (e) Triple helix: a side view for R_{NT}/R_{NP} = 2.0 and P_z = 0.448 MPa. (f1−f6) Quasi-1D ordered structure. (f1) Cross-line close-packed Q1D crystal: The top panel is a top view of only the solvent. The middle panel is a top view. The bottom panel is a side view for R_{NT}/R_{NP} = 2.0 and P_z = 0.251 MPa. (f2) Triangle close-packed Q1D crystal: The top panel is a top view of only the solvent. The middle panel is a top view. The bottom panel is a side view for R_{NT}/R_{NP} = 2.5 and P_z = 0.161 MPa. (f3) Square close-packed Q1D crystal: The top panel is a top view of only solvent. The middle panel is a top view. The bottom panel is a side view for R_{NT}/R_{NP} = 2.5 and P_z = 0.537 MPa. (f4) Coexistence of close-packed crystal and helical sheath: a side view showing the orientation of JNPs in different colors for R_{NT}/R_{NP} = 2.5 and P_z = 0.967 MPa. (f5) Heptagonal crystal with a central JNP chain: The top panel is a top view of only the solvent. The middle panel is a top view. The bottom panel is a side view for R_{NT}/R_{NP} = 3.0 and P_z = 0.877 MPa. (f6) Helical octahedron crystal: The upper panel is a top view of only the orientational vectors. The upper-middle panel is a top view of only the solvent. The lower-middle panel is a top view. The lower panel is a side view for R_{NT}/R_{NP} = 3.167 and P_z = 0.609 MPa. (g) Q1D amorphous phase: The top panel is a top view, and the bottom panel is a side view for R_{NT}/R_{NP} = 3.0 and P_z = 0.147 MPa.

For R_{NT}/R_{NP} = 1.5, the JNPs have more freedom to rotate within the nanotube due to the entropic factor. Hence, the orientational vector of JNPs exhibits random configurations (Figure 3a2), and thus $S \sim 0$. JNPs can interact more strongly with each other through the hydrophobic caps while hydrophilic bands tend to be in contact with the wall. As a result, a zigzag polymer (Figure 3b2) is formed for $P_z > 0.08$ MPa, and S is ~1. In contrast, under the strong confinement R_{NT}/R_{NP} = 1.1 and relatively high pressure $P_z \sim 0.4$ MPa, a straight polymer chain (Figure 3b1) is formed for which S decreases slightly from 1.

Again, the Q1D liquid phase is observed for $R_{NT}/R_{NP} \geq 2.0$ and $P_z < 0.08$ MPa (Figure 3c), as in the case of the hydrophobic nanotube, although here the S value is larger. When $P_z > 0.08$ MPa, the polymer chain begins to crook. For $P_z > 0.1$ MPa, helical structures are formed at R_{NT}/R_{NP} = 2.0. However, orientation of the JNPs is quite different from that in the hydrophobic nanotube. When P_z ~0.15 MPa, a double helix is formed (Figure 3d). The triple-helix morphology (Figure 3e) occurs at $P_z \sim 0.35$ MPa. In the pressure range of 0.15−0.35 MPa, an ordered structure arises as an intermediate structure (Figure 3f1) between the double- and triple-helix. This new structure is shown in Figure 2f1, where JNPs are stacked pairs on top of each other in the axial direction with neighboring pairs forming a 90° angle. In the top view of the new structure, there are four domains, whereas there are eight domains for the counterpart in the hydrophobic nanotube. Again, we name this structure the cross-line close-packed Q1D crystal.

For $R_{NT}/R_{NP} \geq 2.5$, two close-packed Q1D crystals are also observed, one at $P_z \sim 0.15$ (Figure 3f2) and another at 0.5 MPa (Figure 3f3). The former exhibits staggered triangle structure, while the latter exhibits a staggered square structure. In other words, the two staggered layers repeat periodically in the axial direction. Hereafter, we name the former a triangle close-packed Q1D crystal and the latter a square close-packed Q1D crystal. Between the two layers, there is a six-coordinate interstitial site, namely, an octahedral cavity. Note that the two Q1D crystal structures are not strictly close-packed due to the solvent occupation of the central region in the axial direction. As P_z further increases, a helical sheath is formed where JNPs are bonded with one another through the hydrophobic caps. The coexistence of a close-packed crystal and helical sheath is shown in Figure 3f4. The specific-volume and the potential-energy sequences as a function of P_z at R_{NT}/R_{NP} = 2.5 are shown in Figure S3. The feature of first-order transition is evidenced by the hysteresis in the pressure range P_z = 0.53 to −0.60 MPa.

For $R_{NT}/R_{NP} \geq 2.75$, Q1D amorphous appears in the intermediate range of axial pressure ($0.05 < P_z < 0.4$ MPa) as shown in Figure 3g. A morphology transition from Q1D amorphous to the Q1D ordered structure occurs when $P_z > 0.4$ MPa. For R_{NT}/R_{NP} = 3.0 and $P_z \sim 0.8$, JNPs aggregate into a Q1D heptagonal crystal with a central JNP chain (Figure 3f5). For R_{NT}/R_{NP} = 3.167 and $P_z \sim 0.6$, the system becomes a core−sheath structure where the sheath is composed of staggered hexagons (Figure 3f6). The orientational vector of JNPs is mostly perpendicular to the axial direction, as shown in the top panel of Figure 3f6.

Hydroneutral Wall. In the third series, we investigate the phase behavior of JNP solutions confined to the so-called hydroneutral nanotubes. The inner wall of the hydroneutral nanotube favors neither the solvent nor the hydrophobic or hydrophilic section of JNP. In Figure 4, we show a qualitative phase diagram of the system, including representative snapshots of equilibrium morphologies as insets.

For $R_{NT}/R_{NP} < 1.7$ and relatively low P_z, single-file dispersion (Figure 4a) is observed, while a polymer chain is observed at higher axial pressure. The orientational vector of JNPs is perpendicular to the axial direction, and $S \sim 0.5$. Figure 4b1 and b2 show the polymer chain at R_{NT}/R_{NP} = 1.5 and P_z = 0.072 and R_{NT}/R_{NP} = 2.0 and P_z = 0.054, respectively. The polymer chain in Figure 4b1 looks similar to that in Figure 2b.

dx.doi.org/10.1021/ct3007748 | J. Chem. Theory Comput. 2013, 9, 179−187

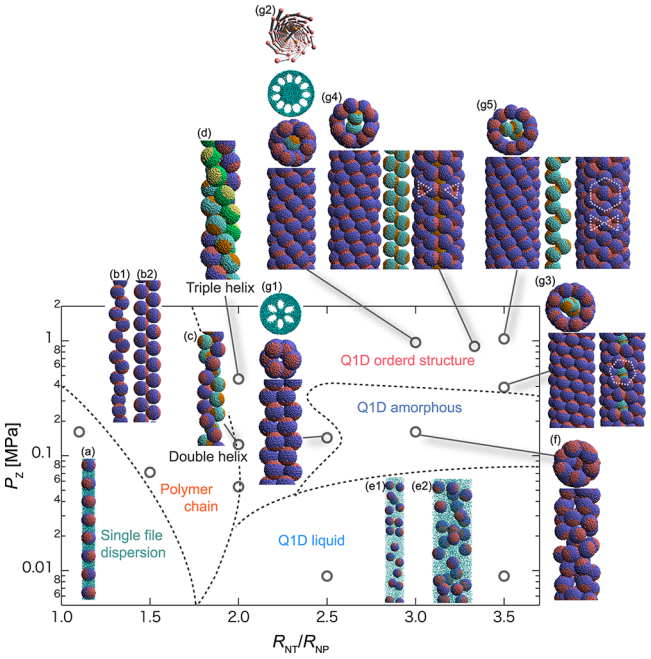

Figure 4. A schematic phase diagram for the triblock JNP solution confined to hydroneutral nanotubes. Insets a–f: Representative snapshots of equilibrium morphologies of the triblock JNP solution (nanotube not shown in the figure). (a) Single file dispersion: a side view for R_{NT}/R_{NP} = 1.1 and P_z = 0.161 MPa. (b1 and b2) Polymer chain: side views for R_{NT}/R_{NP} = 1.5 and P_z = 0.072 MPa, and R_{NT}/R_{NP} = 2.0 and P_z = 0.054 MPa, respectively. (c) Double helix: a side view for R_{NT}/R_{NP} = 2.0 and P_z = 0.107 MPa. (d) Triple helix: a side view for R_{NT}/R_{NP} = 2.0 and P_z = 0.465 MPa. (e1 and e2) Quasi-1D liquid: side views for R_{NT}/R_{NP} = 2.5 and P_z = 0.009 MPa, and R_{NT}/R_{NP} = 3.5 and P_z = 0.009 MPa, respectively. (f) Q1D amorphous phase: The top panel is a top view, and the bottom panel is a side view for R_{NT}/R_{NP} = 3.0 and P_z = 0.161 MPa. (g1–g5) Quasi-1D ordered structure. (g1) Triangle close-packed Q1D crystal: The top panel is a top view of only the solvent. The middle panel is a top view, and the bottom panel is a side view for R_{NT}/R_{NP} = 2.5 and P_z = 0.143 MPa. (g2) Helical octahedron crystal: The upper panel is a top view of only orientational vectors. The upper-middle panel is a top view of only the solvent. The lower-middle panel is a top view. The lower panel is a side view for R_{NT}/R_{NP} = 3.0 and P_z = 0.967 MPa. (g3) Helical octagonal sheath with a defect: The top panel is a top view. The bottom-left panel is a side view. The bottom-right panel is an axially rotated side view for R_{NT}/R_{NP} = 3.5 and P_z = 0.394 MPa. (g4) Helical sheath with a central zigzag polymer core: The top panel is a top view. The bottom-left panel is a side view. The bottom-middle panel is a side view with JNPs in the sheath being excluded. The bottom-right panel is an axially rotated side view for R_{NT}/R_{NP} = 3.333 and P_z = 0.895 MPa. (g5) Helical sheath with a central zigzag polymer core: The top panel is a top view. The bottom-left panel is a side view. The bottom-middle panel is a side view with JNPs in the sheath being excluded. The bottom-right panel is an axially rotated side view for R_{NT}/R_{NP} = 3.5 and P_z = 1.039 MPa.

Moreover, the hydrophobic caps of JNPs in the zigzag double-chain polymer (Figure 4b2) are in contact with the inner wall of the nanotube, indicating that the hydroneutral nanotube is effectively similar to the hydrophobic nanotube in the strong confinement range (R_{NT}/R_{NP} < 2.0). The reason is that hydrophobic caps of JNPs tend to be in contact with the inner wall of the nanotube to reduce the contact area with the solvent. The zigzag double-chain polymer (Figure 4b2) is similar to the central core shown in Figure 2f5. This similarity implies that the central environment inside the hydrophobic nanotube is effectively hydroneutral due to a delicate balance among all forces involved in the central region. Note that when a surfactant solution is confined to a hydrophobic nanotube, the central region may be viewed effectively as a hydrophilic nanotube with a reduced diameter since hydrophobic tails of surfactants are preferred to be adsorbed on the inner surface of the hydrophobic nanotube. As such, the head groups of the surfactants are all pointing toward the central region of the nanotube.[40] Hence, the surfactant which is small and soft can fill interstices by changing shape with greater freedom than the JNPs. In fact, the inner surface of the JNP sheath is much rougher than the surfactant monolayer. Therefore, the effect of packing is more dominant in the JNP system than the surfactant system.

For R_{NT}/R_{NP} = 2.0, a double helix (Figure 4c) is observed at $P_z \sim 0.1$, and for $P_z > 0.2$ a triple helix is the preferred morphology (Figure 4d). The formation of the helices reflects a competition between the confinement and the tendency of dispersion. Without the nanotube confinement, the helices are expected to separate into a number of individual polymer chains at relatively high pressure.

For $R_{NT}/R_{NP} > 2.0$, the Q1D liquid phase emerges at relatively low axial pressure, $P_z < 0.08$ MPa (Figure 4e1, e2), while the Q1D amorphous phase emerges in the intermediate pressure range, $0.08 < P_z < 0.5$ MPa (Figure 4f). For $P_z > 0.5$ MPa, several Q1D ordered structures are formed, depending on the value of R_{NT}/R_{NP} (Figures 4g1–g5). For R_{NT}/R_{NP} = 2.5 and $P_z \sim 0.15$, the triangle close-packed Q1D crystal is formed, where the orientational vector of JNPs lines up in the axial direction (Figure 4g1). For R_{NT}/R_{NP} = 3.5 and $P_z \sim 0.4$ MPa, a Q1D crystal structure with a helical octagonal sheath and a polymer core arises but with the sheath containing defects, as shown in Figure 4g3. Figure 4g4 and g5 show the helical sheath with a zigzag polymer core at R_{NT}/R_{NP} = 3.333 and $P_z \sim 0.9$ MPa and R_{NT}/R_{NP} = 3.5 and $P_z \sim 1.0$ MPa, respectively. In the former structure, some JNPs in the sheath form a triangular bond (see white dashed line in Figure 4g4) like a node formed in the initial process of a Kagome lattice crystallization. In the latter, some parts of the sheath exhibit a hexagonal pattern (see white dashed line in Figure 4g5). Also, there are two triangular bonds in the hexagonal lattice, like a partial unit in the Kagome lattice. These results suggest that many main features in the self-assembled JNPs can be manifested in the hydroneutral nanotube. This is because the forces exerted on the inner wall of the nanotube are the same regardless of hydrophobic and hydrophilic sections of JNPs, and there is no favored direction for the orientational vector.

Description of a Universal Feature: Assembly Map. The overall similarity in the phase behavior shown in three phase diagrams (Figures 2–4) implies certain universal features for the JNPs confined to nanotubes, regardless of the chemical nature of the inner wall. We find that one universal feature can be illustrated by an assembly map, as shown in Figure 5. Here, the vertical axis is the coordination number N_C of JNPs, and the horizontal axis is the ratio R_{NT}/R_{NP}. Representative equilibrium morphologies shown in Figures 2–4 are marked as data points in the assembly map. The three types of inner wall are reflected by the shapes of data points: a circle for a hydrophobic nanotube, a square for a hydrophilic nanotube, and a triangle for a hydroneutral nanotube. Data points are also colored and grouped together according to the assemblies: Green represents single-file dispersion. Orange represents a polymer chain. Blue represents Q1D liquid. Dark blue represents Q1D amorphous.

dx.doi.org/10.1021/ct3007748 | J. Chem. Theory Comput. 2013, 9, 179–187

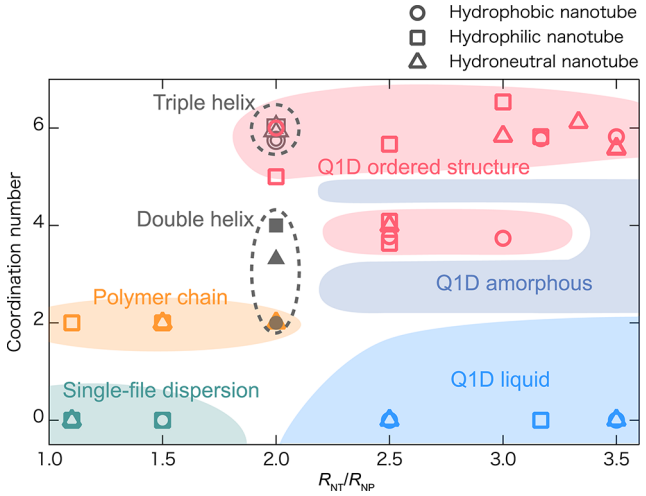

Figure 5. A schematic assembly map for the triblock JNP solutions confined to three different nanotubes. The vertical axis is the average coordination number of JNP, and the horizontal axis is the ratio R_{NT}/R_{NP}. Representative snapshots of the equilibrium morphologies shown in Figures 2, 3, and 4 are marked, where a circle represents structures observed in a hydrophobic nanotube, a square represents structures in a hydrophilic nanotube, and a triangle represents structures in a hydroneutral nanotube. Abbreviations: Q1D, quasi-one-dimensional.

Red represents Q1D ordered structure. In addition, double- and triple-helices are represented by filled gray points and double gray points, respectively.

Figure 6 displays a roadmap for increasing the coordination number in three types of nanotubes. The bottom panels in

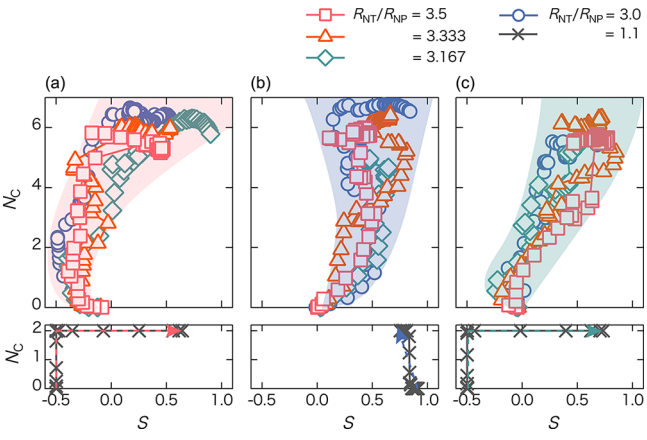

Figure 6. A schematic roadmap suggested for increasing the coordination number (N_C) of JNP in different nanotubes: (a) hydrophobic, (b) hydrophilic, and (c) hydroneutral nanotube. The vertical axes are the coordination number, and the horizontal axes are orientational order parameter S. Bottom panels show processes under strong confinement conditions (R_{NT}/R_{NP}= 1.1). Red, blue, and green shaded areas represent JNPs in wider ($R_{NT}/R_{NP} \geq 3.0$) hydrophobic, hydrophilic, and hydroneutral nanotube, respectively. Equilibrium structures in R_{NT}/R_{NP} = 3.5, 3.333, 3.167, 3.0, and 1.1 are marked in square, triangle, rhombus, circle, and cross, respectively.

Figure 6 show processes under a strong confinement limit (R_{NT}/R_{NP} = 1.1). Red, blue, and green shaded areas in the top panels of Figure 6 represent JNP solution in a relatively wide ($R_{NT}/R_{NP} \geq 3.0$) hydrophobic, hydrophilic, and hydroneutral nanotube, respectively. The vertical axis is the coordination number N_C, and the horizontal axis is the orientational order parameter S. (Note: with increasing the axial pressure, the coordination number increases as well, as shown in Figure S4.)

First, under strong confinement ($R_{NT}/R_{NP} \leq 1.5$), there is little space for JNPs to pass by each other along the axial direction. Therefore, the maximum value of N_C is two. At low P_z, JPNs are dispersed single-file. As P_z increases, JNPs are bonded together, forming a polymer chain. In any case, JNPs always interact with the inner wall because their radius of JNP is close to that of the nanotube. In a hydrophobic nanotube, the hydrophobic caps of JNPs are in contact with the inner wall of the nanotube, while in the hydrophilic nanotube, the hydrophilic band of JNPs is in contact with the inner wall. The corresponding S value in the hydrophobic and hydrophilic nanotube is ∼−0.5 and 1.0, respectively.

In the hydrophobic nanotube, further increasing P_z results in a stronger interaction among JNPs so that N_C increases to 2. In this case, S is ∼−0.5 because hydrophobic caps of JNPs are in contact with the inner wall of the nanotube to reduce a contact area between the hydrophobic caps and solvent. As P_z further increases, S changes to ∼1.0 due to the stronger interaction among JNPs than that between JNP and the wall (see the red arrow in Figure 6a). The case of the hydroneutral nanotube is the same as that of the hydrophobic nanotube due to similarity of the contact area with the solvent. On the other hand, the S value in the case of the hydrophilic nanotube exhibits little change during the transition from the single-file dispersion to a polymer chain.

Next, for nanotubes with a larger radius ($R_{NT}/R_{NP} \geq 2.0$), N_C becomes more than two as JNPs can form various assemblies in all three types of nanotubes. In fact, R_{NT}/R_{NP} = 2.0 can be viewed as a critical value to achieving $N_c > 2$. As seen in Figures 2d,e, 3d,e, and 4c,d, double or triple helix structures emerge at R_{NT}/R_{NP} = 2.0 despite different orientations of JNPs. Note also that the double helix here is similar to a rope-like micelle in our previous simulation of confined surfactants in a hydrophilic nanotube[40] where two to three threadlike micelles intertwine. Nevertheless, the formation of a helix depends more strongly on R_{NT}/R_{NP}, while the orientational vector of JNPs is affected by the chemical nature of the nanotube. All three double helices are similar to each other, but the local-bond configuration and orientation of JNPs differ substantially. For the double-helix in the hydrophobic nanotube, one of the JNP hydrophobic caps is in contact with the inner wall, while the other cap is in contact with neighbor particles. The double-helix can be also viewed as a periodic twist of the zigzag double-chain polymer. In the hydrophilic nanotube, JNPs connect one another to form the polymer chain whose hydrophilic band is in contact with the inner wall. Two polymer chains are intertwined so that the double-helix is formed inside the hydrophilic nanotube. The orientational order parameter is nearly 1.0, and N_C is 4: two from direct contact between two JPNs in a polymer chain, with another two from pulling another polymer chain. The helix in the hydroneutral nanotube, however, is formed due to a delicate balance between inter-JNPs and JNP/solvent interactions. Here, triangular bonds are formed among JNPs while hydrophobic caps of JNPs are in contact with the wall. For this structure, N_C and S were ∼3.3 and ∼−0.26, respectively. These results show that the condition and process for the formation of helices are dependent on the chemical nature of the nanotube.

Similar behavior has been seen in the liquid crystal phase. For example, a liquid crystal with helical variation in orientation is known as the cholesteric liquid crystal, which can be used in switchable optical devices using characteristic optical-pitch.[46,47]

dx.doi.org/10.1021/ct3007748 | J. Chem. Theory Comput. 2013, 9, 179−187

The JNPs may be also used to control the orientation of nanoplatforms. Our simulation suggests that the helix structure can be made at relatively low pressure in a hydrophobic nanotube. For tripe helices, N_C (~ 6) is nearly the same in all nanotubes, but S is dependent on the chemical nature of the nanotube, as in the case of the double helix. Orientational order parameters in the case of hydrophobic, hydrophilic, and hydroneutral nanotubes are −0.424, 0.832, and 0.098, respectively. In our previous study of self-assembly of surfactants, the helix structure is emerged in the hydrophilic nanotube. Because of chain-like bonding, the polymer chain in the JNP system is formed on every nanotube, but the threadlike micelle is formed only on the hydrophilic nanotube in the surfactant solution system.

The Q1D liquid phase arises in the nanotube with a larger diameter, i.e., for $R_{NT}/R_{NP} > 2$. In the liquid phase, typically, $N_c < 2$, and JNPs can move somewhat freely in the nanotube. But the motion of JNPs is not isotropic; the diffusion constant in the radial direction is about 10 times smaller than in the axial direction. The orientational vectors of JNPs are random, and thus S is nearly zero, regardless of the nanotube (Figure 6). For the Q1D amorphous phase, N_C increases, i.e., $2 < N_C < 4$. Here, JNPs show little motion (solid-like) without long-range order. The orientational order parameter in this phase exhibits a certain trend but depending on the chemical interaction between the JNP and inner wall of nanotube.

All Q1D structures shown in Figures 2f2,f3, 3f2,f3, and 4g1 exhibit $N_C \sim 4$. Every Q1D ordered structure entails a bilayer unit. One layer is either triangle or square, while the two nearest-neighbor layers on top and bottom are located in a stagger fashion. The bilayer unit repeats periodically in the axial direction. For theses Q1D close-packed structures, $N_C \sim 4$. The structure shown in Figure 3f1 also has the same pattern as the Q1D ordered structures. However, this structure has $N_C = 5$, a special case between that of the double- and triple-helix in the hydrophilic nanotube. This ordered structure no longer exists with further increases of N_C. When $N_C \sim 6$, a new ordered structure arises, e.g., those shown in Figures 2f5, 3f6, and 4g2. Here, the helical octahedron crystal is formed as the outer sheath. The orientational vector of JNPs tends to fit a circumferential length due to the strong confinement. Here, the confinement effect is much stronger than the interaction among JNPs. As such, S exhibits a broad range of values, regardless of the chemical nature of nanotubes (Figure 6). All of these results indicate that highly ordered structures tend to form in the nanotube when N_C is a multiple of 2.

CONCLUSION

In conclusion, our simulation reveals a wealth of self-assembly morphologies for the triblock JNP solution confined to different nanotubes. Major driving forces for the self-assembly process include hydrophobic interaction and hydrophilic interaction among JNP, the solvent, and the inner wall of the confining nanotube. One of the key parameters that can control the morphology is the ratio R_{NT}/R_{NP}, which measures the degree of confinement. Another key parameter is the axial pressure P_z. When $R_{NT}/R_{NP} < 2.0$ (under strong confinement), morphologies are quite simple, i.e., either a single-file dispersion or a polymer chain, depending on P_z. The orientational vector of JNPs can be strongly influenced by the chemical nature of the nanotube. When $R_{NT}/R_{NP} > 2.0$, rich morphologies can arise; for example, double-helix and triple-helix are both observed for $R_{NT}/R_{NP} = 2.0$. Importantly, we find that highly ordered structures tend to form when the N_C is a multiple of 2. In many cases, the orientational vector and self-assembly behavior of JNPs can be qualitatively assessed on the basis of the chemical nature of the nanotube. Our simulation offers a theoretical guide to control morphologies of the self-assembled JNPs, a novel system that may find applications in nanofluidic devices or for nanopatterning.

ASSOCIATED CONTENT

Supporting Information

Snapshot of a Kagome lattice structure and plots of time evolution of the fraction of discrete nanoparticles, strings, and triangular bonding; density profiles of hydrophobic, hydrophilic, and solvent beads; and plots of specific volume, potential energy, and coordination number as a function of the axial pressure are collected. This material is available free of charge via the Internet at http://pubs.acs.org/.

AUTHOR INFORMATION

Corresponding Author

*E-mail: arai@mce.uec.ac.jp; yasuoka@mceh.keio.ac.jp; xzeng1@unl.edu.

Notes

The authors declare no competing financial interest.

ACKNOWLEDGMENTS

K.Y. was supported by JSPS KAKENHI Grant Number 24360084. X.C.Z. was supported by grants from the NSF (CBET-1036171 and CBET-1066947) and ARL (W911NF1020099).

REFERENCES

(1) Holtz, J. H.; Asher, S. A. Polymerized Colloidal Crystal Hydrogel Films as Intelligent Chemical Sensing Materials. *Nature* **1997**, *389*, 829−832.

(2) Bigioni, T. P.; Lin, X. M.; Nguyen, T. T.; Corwin, E. I.; Wittern, T. A.; Jaeger, H. M. Kinetically Driven Self-Assembly of Highly Ordered Nanoparticle Monolayers. *Nat. Mater.* **2006**, *5*, 265−270.

(3) Cheng, W.; Wang, J. J.; Jonas, U.; Fytas, G.; Stefanou, N. Observation and Tuning of Hypersonic Bandgaps in Colloidal Crystals. *Nat. Mater.* **2006**, *5*, 830−836.

(4) Nykypanchuk, D.; Maye, M. M.; van der Lelie, D.; Gang, O. DNA-Guided Crystallization of Colloidal Nanoparticles. *Nature* **2008**, *451*, 549−552.

(5) Redl, F. X.; Cho, K. S.; Murray, C. B.; O'Brien, S. Three-Dimensional Binary Superlattices of Magnetic Nanocrystals and Semiconductor Quantum Dots. *Nature* **2003**, *423*, 968−971.

(6) Tikhomirov, G.; Hoogland, S.; Lee, P. E.; Fischer, A.; Sargent, E. H.; Kelley, S. O. DNA-Based Programming of Quantum Dot Valency, Self-Assembly and Luminescence. *Nat. Nanotechnol.* **2011**, *6*, 485−490.

(7) Glotzer, S. C.; Solomon, M. J. Anisotropy of Building Blocks and Their Assembly into Complex Structures. *Nat. Mater.* **2007**, *6*, 557−562.

(8) Chen, Q.; Diesel, E.; Whitmer, J. K.; Bae, S. C.; Luijten, E.; Granick, S. Triblock Colloids for Directed Self-Assembly. *J. Am. Chem. Soc.* **2011**, *133*, 7725−7727.

(9) Kraft, D. J.; Ni, R.; Smallenburg, F.; Hermes, M.; Yoon, K.; Weitz, D. A.; van Blaaderen, A.; Groenewold, J.; Dijkstra, M.; Kegel, W. K. Surface Roughness Directed Self-Assembly of Patchy Particles into Colloidal Micelles. *Proc. Natl. Acad. Sci. U. S. A.* **2012**, *109*, 10787−10792.

(10) Damasceno, P. F.; Engel, M.; Glotzer, S. C. Predictive Self-Assembly of Polyhedra into Complex Structures. *Science* **2012**, *337*, 453−457.

(11) Burda, C.; Chen, X.; Narayanan, R.; El-Sayed, A. Chemistry and Properties of Nanocrystals of Different Shapes. *Chem. Rev.* **2005**, *105*, 1025−1102.
(12) Agarwal, U.; Escobedo, F. A. Mesophase Behaviour of Polyhedral Particles. *Nat. Mater.* **2011**, *10*, 230−235.
(13) Gudiksen, M. S.; Lauhon, L. J.; Wang, J.; Smith, D. C.; Lieber, C. M. Growth of Nanowire Superlattice Structures for Nanoscale Photonics and Electronics. *Nature* **2002**, *415*, 617−620.
(14) Brown, E.; Forman, N. A.; Orellana, C. S.; Zhang, H.; Maynor, B. W.; Betts, D. E.; DeSimone, J. M.; Jaeger, H. M. Generality of Shear Thickening in Dense Suspensions. *Nat. Mater.* **2010**, *9*, 220−224.
(15) Suci, P. A.; Kang, S.; Young, M.; Douglas, T. A. Streptavidin-Protein Cage Janus Particle for Polarized Targeting and Modular Functionalization. *J. Am. Chem. Soc.* **2009**, *131*, 9164−9165.
(16) Cole-Hamilton, D. J. Janus Catalysts Direct Nanoparticle Reactivity. *Science* **2010**, *327*, 41−42.
(17) Jiang, H.-R.; Yoshinaga, N.; Sano, M. Active Motion of a Janus Particle by Self- Thermophoresis in a Defocused Laser Beam. *Phys. Rev. Lett.* **2010**, *105*, 268302.
(18) Chen, Q.; Bae, S. C.; Granick, S. Directed Self-Assembly of a Colloidal Kagome Lattice. *Nature* **2011**, *469*, 381−384.
(19) Chen, Q.; Whitmer, J. K.; Jiang, S.; Bae, S. C.; Luijten, E.; Granick, S. Supracolloidal Reaction Kinetics of Janus Spheres. *Science* **2011**, *331*, 199−202.
(20) Zhang, Z.; Pfleiderer, P.; Schofield, A. B.; Clasen, C.; Vermant, J. Synthesis and Directed Self-Assembly of Patterned Anisometric Polymeric Particles. *J. Am. Chem. Soc.* **2011**, *133*, 392−395.
(21) Romano, F.; Sciortino, F. Two Dimensional Assembly of Triblock Janus Particles into Crystal Phases in the Two Bond per Patch Limit. *Soft Matter* **2011**, *7*, 5799−5804.
(22) Wang, J.-Y.; Wang, Y.; Sheiko, S. S.; Betts, D. E.; DeSimone, J. M. Tuning Multiphase Amphiphilic Rods to Direct Self-Assembly. *J. Am. Chem. Soc.* **2012**, *134*, 5801−5806.
(23) Roh, K. H.; Martin, D. C.; Lahann, J. Biphasic Janus Particles with Nanoscale Anisotropy. *Nat. Mater.* **2005**, *4*, 759−763.
(24) Higuchi, T.; Tajima, A.; Motoyoshi, K.; Yabu, H.; Shimomura, M. Suprapolymer Structures from Nanostructured Polymer Particles. *Angew. Chem., Int. Ed.* **2009**, *48*, 5125−5128.
(25) Lattuada, M.; Hatton, T. A. Synthesis, Properties and Applications of Janus Nanoparticles. *Nano Today* **2011**, *6*, 286−308.
(26) Pawar, A. B.; Kretzschmar, I. Patchy Particles by Glancing Angle Deposition. *Langmuir* **2008**, *24*, 355−358.
(27) Maddox, M. W.; Gubbins, K. E. A Molecular Simulation Study of Freezing/Melting Phenomena for Lennard-Jones Methane in Cylindrical Nanoscale Pores. *J. Chem. Phys.* **1997**, *107*, 9659−9667.
(28) Mashi, R. J.; Joseph, S.; Aluru, N. R.; Jakobsson, E. Anomalously Immobilized Water: A New Water Phase Induced by Confinement in Nanotubes. *Nano Lett.* **2003**, *3*, 589−592.
(29) Koga, K.; Gao, G.; Tanaka, H.; Zeng, X. C. Formation of Ordered Ice Nanotubes inside Carbon Nanotubes. *Nature* **2001**, *412*, 802−805.
(30) Qiao, Y.; Cao, G.; Chen, X. Effects of Gas Molecules on Nanofluidic Behaviors. *J. Am. Chem. Soc.* **2007**, *129*, 2355−2359.
(31) Arai, N.; Yasuoka, K.; Zeng, X. C. Nanochannel with Uniform and Janus Surfaces: Shear Thinning and Thickening in Surfactant Solution. *Langmuir* **2012**, *28*, 2866−2872.
(32) Hoogerbrugge, P. J.; Koelman, J. M. V. A. Simulating Microscopic Hydrodynamics Phenomena with Dissipative Particle Dynamics. *Europhys. Lett.* **1992**, *19*, 155−160.
(33) Espanõl, P.; Warren, P. B. Statical-Mechanics of Dissipative Particle Dynamics. *Europhys. Lett.* **1995**, *30*, 191−196.
(34) Hiyama, M.; Kinjo, T.; Hyodo, S. Angular Momentum Form of Verlet Algorithm for Rigid Molecules. *J. Phys. Soc. Jpn.* **2008**, *77*, 064001.
(35) Spirin, L.; Galuschko, A.; Kreer, T.; Binder, K.; Baschnagel, J. Polymer-Brush Lubricated Surfaces with Colloidal Inclusions under Shear Inversion. *Phys. Rev. Lett.* **2011**, *106*, 168301.
(36) Cigler, P.; Lytton-Jean, A. K. R.; Anderson, D. G.; Finn, M. G.; Park, S. Y. DNA-Controlled Assembly of a NaTl Lattice Structure from Gold Nanoparticles and Protein Nanoparticles. *Nat. Mater.* **2010**, *9*, 918−922.
(37) Park, S. Y.; Lytton-Jean, A. K. R.; Lee, B.; Weigand, S.; Schatz, G. C.; Mirkin, C. A. DNA-Programmable Nanoparticle Crystallization. *Nature* **2008**, *451*, 553−556.
(38) Fedosova, D. A.; Pan, W.; Caswell, B.; Gompper, G.; Karniadakis, G. E. Predicting Human Blood Viscosity in Silico. *Proc. Natl. Acad. Sci. U. S. A.* **2011**, *108*, 11772−11777.
(39) Groot, R. D.; Warren, P. B. Dissipative Particle Dynamics: Bridging the Gap between Atomistic and Mesoscopic Simulation. *J. Chem. Phys.* **1997**, *107*, 4423−4435.
(40) Arai, N.; Yasuoka, K.; Zeng, X. C. Self-Assembly of Surfactants and Polymorphic Transition in Nanotubes. *J. Am. Chem. Soc.* **2008**, *130*, 7916−7920.
(41) Arai, N.; Yasuoka, K.; Koishi, T.; Ebisuzaki, T. Asymmetric Brownian Motor Driven by Bubble Formation in a Hydrophobic Channel. *ACS Nano* **2010**, *4*, 5905−5913.
(42) Jakobsen, A. F. Constant-Pressure and Constant-Surface Tension Simulations in Dissipative Particle Dynamics. *J. Chem. Phys.* **2005**, *122*, 124901. Erratum: Jakobsen, A. F. *J. Chem. Phys.* **2006**, *125*, 029901.
(43) Bai, J.; Wang, J.; Zeng, X. C. Multiwalled Ice Helixes and Ice Nanotubes. *Proc. Natl. Acad. Sci. U. S. A.* **2006**, *103*, 19664−19667.
(44) Melle-Franco, M.; Zerbetto, F. Ejection Dynamics of a Simple Liquid from Individual Carbon Nanotube Nozzles. *Nano Lett.* **2006**, *6*, 969−972.
(45) Groot, R. D.; Rabone, K. L. Mesoscopic Simulation of Cell Membrane Damage, Morphology Change and Rupture by Nonionic Surfactants. *Biophys. J.* **2001**, *81*, 725−736.
(46) Hikmet, R. A. M.; Kemperman, H. Electrically Switchable Mirrors and Optical Components Made from Liquid-Crystal Gels. *Nature* **1998**, *392*, 476−479.
(47) Ha, N. Y.; Ohtuka, Y.; Jeong, S. M.; Nishimura, S.; Suzuki, G.; Takahashi, Y.; Ishikawa, K.; Takezoe, H. Fabrication of a Simultaneous Red-Green-Blue Reflector using Single-Pitched Cholesteric Liquid Crystals. *Nat. Mater.* **2008**, *7*, 43−47.